ADVANCED OPTICAL MATERIALS
www.advopticalmat.de

The Complex Role of Carbon Nitride as a Sensitizer in Photoelectrochemical Cells

*Jingsan Xu, Isaac Herraiz-Cardona, Xiaofei Yang, Sixto Gimenez, Markus Antonietti, and Menny Shalom**

In the last years, enormous attention has been focused on the metal-free semiconductor graphitic carbon nitride (simplified as C_3N_4) with a bandgap of 2.7 eV, which holds a great promise in the fields of electrocatalysis,[1] bioimaging,[2] solar cells,[3] and especially photocatalysis.[4,5] Many approaches were introduced to enhance the photoactivity of C_3N_4, such as doping[6] with different heteroatoms and by surface area increase, usually by hard-templating method.[5] Recently, an easy, safe, and highly effective approach has been developed to promote the photocatalytic activity of C_3N_4, which employs supramolecular precursors for thermal polymerization into C_3N_4. The supramolecular complex is generated by combining different organic compounds (triazine derivatives) in solvents and then assemblies are formed because of noncovalent interactions such as hydrogen bonds. Typically, cyanuric acid-melamine system has been shown to yield preorganized micro/nanostructures and morphologies, and as a result enables the modification of optical and electrical properties of final C_3N_4 product and significant improvement of photoactivity.[7] Moreover, the final material composition can be tuned by the insertion of other molecules (e.g., barbituric acid) into the starting complex.

As stated before, C_3N_4 features good stability over high temperature and corrosive chemical environments.[8] C_3N_4 has been frequently used in combination with other semiconductor materials, such as MoS_2,[9] In_2O_3,[10] and Ag_3PO_4,[11] for better light harvesting. When the chemistry is successfully executed, heterojunctions are formed between C_3N_4 and the other component, which improve the charge separation process and the overall performance. However, while the high activity of C_3N_4 as photocatalyst is well understood and studied, its performance in photoelectrochemical cells (PEC) remained low due to a more complicate charge separation/transport process. In order to promote PEC performance, uniform, continuous, and well-attached thin film electrodes should be produced. Furthermore, it is crucial to better understand the photophysical properties and the chemical interactions of carbon nitride materials in such systems.

Herein, we carefully studied the chemical interactions alongside the photophysical properties of TiO_2/C_3N_4 in a model photoelectrochemical cell. A TiO_2/C_3N_4 hybrid thin film was prepared by an in situ vapor-transport growth mode, using cyanuric acid-melamine (CM) or cyanuric acid-melamine-barbituric acid (CMB) supramolecular complexes as the precursor (labeled here as TiO_2/CM and TiO_2/CMB, respectively). The hybrid materials were characterized using a range of techniques (summarized in Table S1, Supporting Information). After thermal polymerization, the 20-nm TiO_2 nanoparticles were uniformly coated with 3–5 nm of C_3N_4 layers. The TiO_2/C_3N_4 system showed unique electronic coupling, leading to a greatly modified electronic structure and enhanced optical absorption. Consequently, the visible-light driving photocurrent was raised by ≈30 times for TiO_2/C_3N_4 as compared with a comparable pristine TiO_2 cell.

The material growth approach is developed on the basis of previous reports on improving photoactivities of C_3N_4[12] with certain modifications, as schematically shown in **Figure 1**. First, mesoporous TiO_2 thin film on fluorine-doped tin oxide (FTO) glass was prepared by a doctor-blade method using commercial paste followed by air-annealing. Second, CM or CMB precursor was placed on top of the substrate, fully covering the TiO_2 film. Then the system was put in crucible, capped, and heated in nitrogen (detailed information is given in the Supporting Information).

The X-ray diffraction (XRD) patterns of the substrates are shown in Figure S1 (Supporting Information). Compared with bare FTO, the additional diffraction peaks confirmed the formation of TiO_2 film, which was mainly composed of the anatase phase. After the growth of C_3N_4 layers, the TiO_2 phase remained unchanged and no impurity peaks from, e.g., TiN or TiC were detected. It is noticeable that the diffraction patterns of C_3N_4 layer cannot be resolved because of its thinness (as shown in **Figure 2**) and the high crystallinity of TiO_2 and FTO. However, the Fourier transform infrared spectroscopy spectra (Figure S1b, Supporting Information) of TiO_2/CM and TiO_2/CMB clearly demonstrated the vibration peaks at 1200–1650 cm^{-1}, which correspond to the typical stretching modes of C–N heterocycles that implied the C_3N_4 formation. The invisibility of triazine peak at ≈810 cm^{-1} was due to the overlapping with the broad strong absorption band of TiO_2 located in the range of 550–800 cm^{-1}. Further support was given by the elemental analysis results, showing C/N molar ratio of 0.71 for TiO_2/CM, which is a typical value for normal C_3N_4 samples.[13] The ratio increased to 0.90 for TiO_2/CMB, due to the incorporation of barbituric acid molecules into the precursor. The Raman spectra (Figure S1c, Supporting Information) shows the bands at 193, 392, 512, and 635 cm^{-1} corresponding to the characteristic $E_{g(1)}$, $B_{1g(1)}$, $A_{1g} + B_{1g(2)}$ doublet, and $E_{g(2)}$ mode of anatase TiO_2, respectively. The $E_{g(1)}$ and $B_{1g(1)}$ modes are O–Ti–O bending

Dr. J. Xu, Dr. X. Yang, Prof. M. Antonietti. Dr. M. Shalom
Department of Colloid Chemistry
Max Planck Institute of Colloids and Interfaces
Potsdam 14424, Germany
E-mail: Menny.Shalom@mpikg.mpg.de
Dr. I. Herraiz-Cardona, Dr. S. Gimenez
Departament de Física
Photovoltaics and Optoelectronic Devices Group
Universitat Jaume I, Castelló 12071, Spain

DOI: 10.1002/adom.201500010

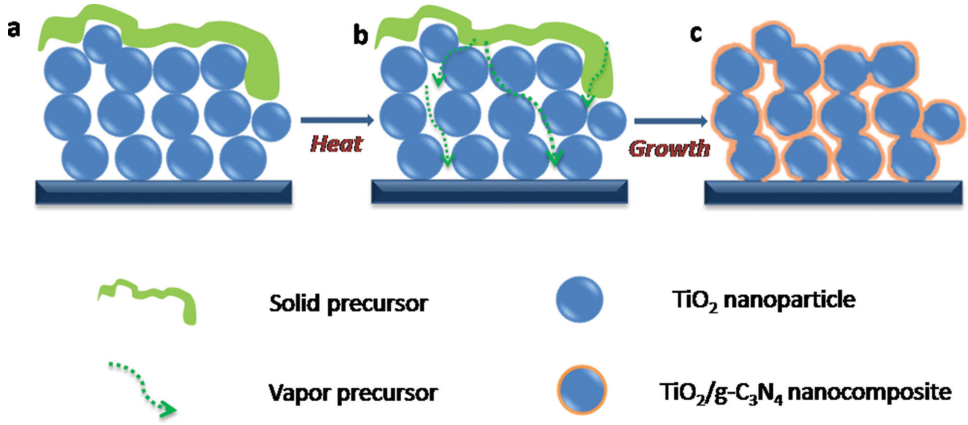

Figure 1. Schematic drawing of the suggested growth process of TiO_2/C_3N_4 thin films.

vibrations while A_{1g} + $B_{1g(2)}$ and $E_{g(2)}$ are Ti–O stretching vibrations.[14] The spectra demonstrated that after C_3N_4 growth the intensity of $E_{g(1)}$ mode was significantly increased and the peak showed slight blue shift, meaning the enhancement of the bending vibration. On the contrary, A_{1g} and $E_{g(2)}$ modes were broadened and shifted to lower wavenumbers, suggesting the increasing of lattice disorder and weakening of the stretching vibrations. The structure evolution of TiO_2 indicated the strong interaction between TiO_2 and C_3N_4, as discussed in more detail later in this manuscript.

Atomic force microscopy was employed to characterize the surface of the TiO_2 and TiO_2/C_3N_4 substrates (Figure S2, Supporting

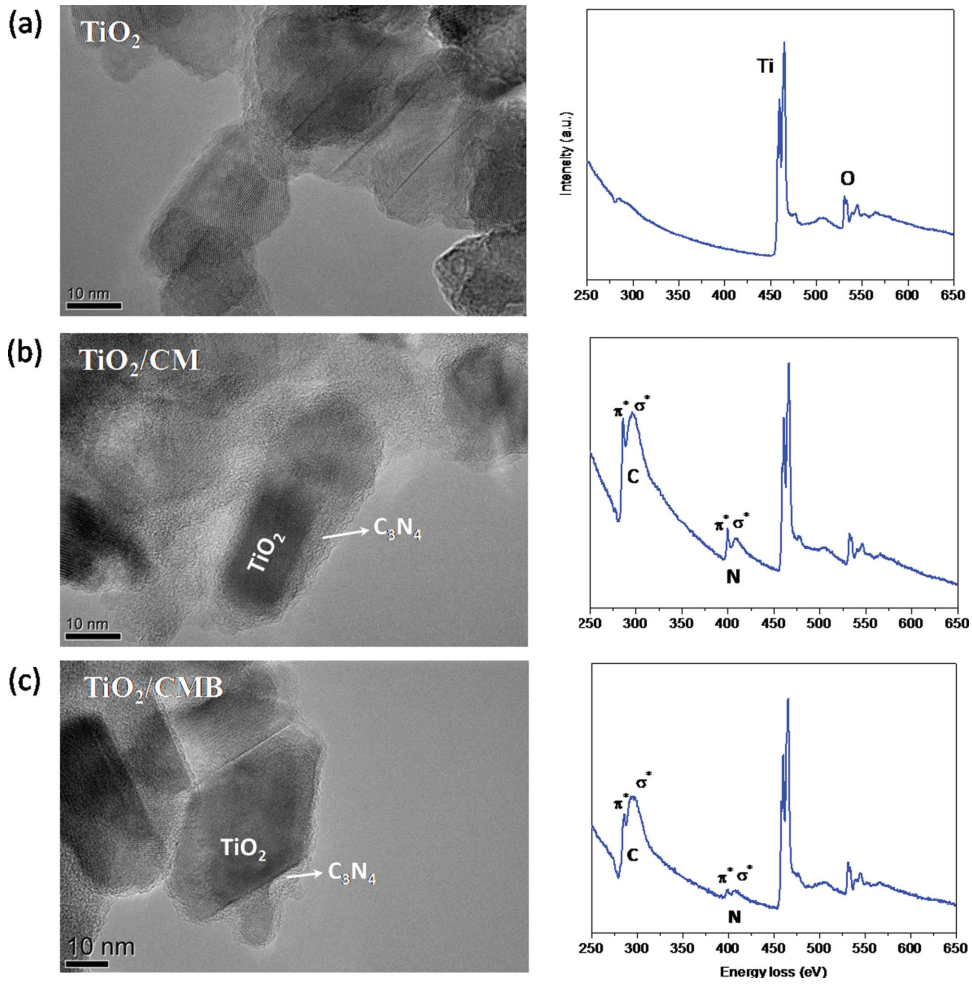

Figure 2. HRTEM image and EELS spectrum of a) pristine TiO_2, b) TiO_2/CM, and c) TiO_2/CMB.

Adv. Optical Mater. **2015**,
DOI: 10.1002/adom.201500010

Information). The morphology and roughness of the substrates were not changed after thermal polymerization (with CM or CMB), e.g., no generation of disordered layers on top was found as reported before.[12,15] The cross-section scanning electron microscopy images also confirmed the absence of extra top layer (Figure S3a, Supporting Information) and only the mesoporous structure of the primary TiO_2 film was observed (Figure S3b,c, Supporting Information). On the contrary, it is very interesting to find out that the TiO_2 nanoparticles were uniformly coated by a thin C_3N_4 layer (3–5 nm), as illustrated by high-resolution transmission electron microscopy (HRTEM) images in Figure 2a. Further evidence of the successful C_3N_4 deposition is given by the electron energy loss spectroscopy (EELS) spectra (Figure 2b). Compared with pristine TiO_2, TiO_2/CM and TiO_2/CMB show the transitions of $1s \rightarrow \pi^*$ and $1s \rightarrow \sigma^*$ in both carbon *K* edge and nitrogen *K* edge. More importantly, the relative intensities of the two transitions (the $1s \rightarrow \pi^*$ transition peaks are very sharp and intense for TiO_2/CM and TiO_2/CMB) demonstrated that the outer layers of the TiO_2/C_3N_4 nanoparticles exclusively consisted of sp^2 hybridized carbon and nitrogen atoms,[16] which further proves the thin layers are composed of carbon nitride. Corresponding selected area electron diffraction patterns illustrates that the C_3N_4 does not have obvious impact on the crystallinity of the TiO_2 nanoparticles (Figure S4, Supporting Information). It is worth noting that we randomly studied ≈10 different spots and we found that all the TiO_2 nanoparticles were coated with C_3N_4 (Figure S5, Supporting Information). In addition, line-scanning energy-dispersive X-ray spectroscopy shows that the nitrogen and carbon contents remain constant across the TiO_2/C_3N_4 film (Figure S3d, Supporting Information). Therefore, it is reasonable to assume that the growth of C_3N_4 took place all across the TiO_2 film. Besides, we found that the CM complex (with and without the TiO_2) did not show a liquid-phase intermediate up to 500 °C (Figure S6, Supporting Information), such that no liquid would penetrate into the TiO_2 thin film during the growth. Given these facts as well as the thickness (≈7 µm) and the mesoporous structure of the TiO_2 film, we can suppose that during the heating process an in situ vapor-transport growth of the C_3N_4 layers occurred. Specifically, sublimation of the CM precursor would be triggered at elevated temperature in the sealed crucible (around 430 °C based on TG-DSC curves, Figure S6b, Supporting Information) and the resulted vapor precursor can transport downward to the TiO_2 substrate driven by concentration gradient. This process is followed by redeposition at the TiO_2 nanoparticles driven by surface energy minimization, as schemed in Figure 1b. Afterwards, thermal polymerization of the precursor towards C_3N_4 occurred on the surface of the TiO_2 nanoparticles with further temperature increase (Figure 1c) and the phase transformations of CM precursor were monitored by XRD measurement (Figure S6d–g, Supporting Information). The growth could have been terminated by several reasons: (1) the oxide surfaces are preferentially coated by C_3N_4 due to surface energy effects; this effect levels off at about 5-nm thickness; (2) the transport of the vapor as well as the thickening of C_3N_4 layer is slowed down or even prohibited because of space limitations.

The chemical states of the material systems were investigated by X-ray photoelectron spectroscopy (XPS), (**Figure 3**a,b). The pristine TiO_2 substrate showed typical binding energies of 458.4 and 529.6 eV for Ti $2p_{3/2}$ and O 1*s*. After carbon nitride growth the Ti $2p_{3/2}$ and O 1*s* peaks shifted to higher binding energies

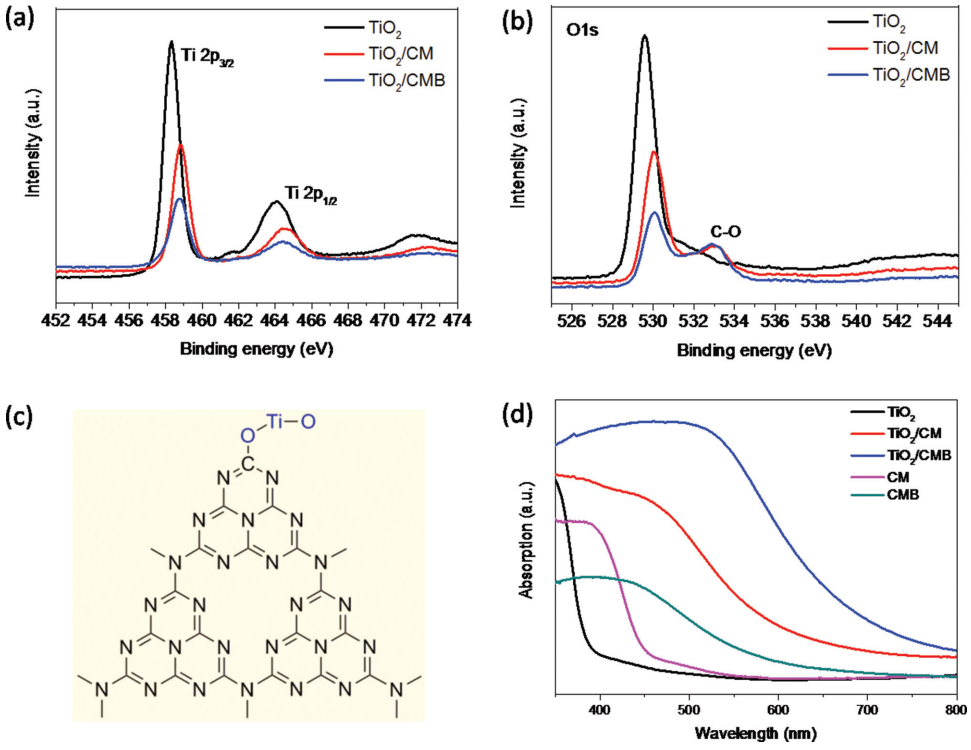

Figure 3. a) Ti 2*p* and b) O 1*s* XPS spectra, c) schematic chemical structure of TiO_2/C_3N_4 and d) UV–vis absorption spectra of the TiO_2, TiO_2/CM, TiO_2/CMB substrates, and C_3N_4 powders made from pure CM and CMB.

(458.8 and 530.0 eV, respectively). Significantly, the binding energy of Ti–O–C bonding appears at 532.8 eV in the O 1*s* spectrum (Figure 3b). In addition, the C 1*s* spectrum also clearly shows the C–O bonding at 286.7 eV (Figure S7a, Supporting Information), implying the formation of direct electronic coupling between TiO_2 and C_3N_4, which is responsible for the positive shifts of the Ti $2p_{3/2}$ and the O 1*s* peaks because C_3N_4 acts apparently as a strong electron withdrawing group on the TiO_2 surface. Interestingly, this kind of chemical interaction between TiO_2 and C_3N_4 has not been reported previously although a few TiO_2/C_3N_4 composites were prepared,[17,18] indicating the peculiarity of the in situ vapor transport based growth mode of C_3N_4 on mesoporous TiO_2. In addition, the shift of Ti $2p_{3/2}$ peak to higher binding energies implies that nitrogen doping of TiO_2 during the synthesis could be excluded. Moreover, no Ti–C or Ti–N coordination schemes were detected. We note that free C_3N_4 powders made from CM complex did not show any C–O or C=O bonds (Figure S8, Supporting Information), indicating that the generation of C–O bonding is due to the chemical coupling between TiO_2 and C_3N_4 (Figure 3c).

The N 1*s* XPS spectra are shown in Figure S7a (Supporting Information) and the spectrum of TiO_2/CM was fitted into several binding energies (Figure S7c, Supporting Information). The main peak at 398.7 and 399.8 eV can be attributed to the C–N–C coordination and tertiary nitrogen $N–(C)_3$ groups, respectively.[13] The peak at 400.8 eV resulted from the bonding of C–N–H. The C 1*s* spectrum is shown in Figure S7b (Supporting Information) (fitted curve in Figure S7d, Supporting Information), demonstrating the occurrence of C–N–C group with binding energy at 288.3 eV. The N and C spectrum corresponds well with that of typical C_3N_4 samples.

The UV–vis absorption spectra are shown in Figure 3d. The pristine TiO_2 substrate showed a clear absorption edge at 400 nm, corresponding to the bandgap of 3.1 eV of anatase. After thermal polymerization with the supramolecular precursors, the absorption of TiO_2/CM was strongly enhanced in the visible-light range, and the edge shifted to ≈600 nm and beyond for TiO_2/CMB (see also Figure S9, Supporting Information). It is important to note that corresponding to the XPS measurements, the optical absorption is fundamentally different from that of C_3N_4 made from pure CM and CMB, N-doped or C-decorated TiO_2[19] and conventional TiO_2/C_3N_4 composites. Given the promotion of light absorption, we investigated the photocurrents (**Figure 4**a) of the substrates under visible

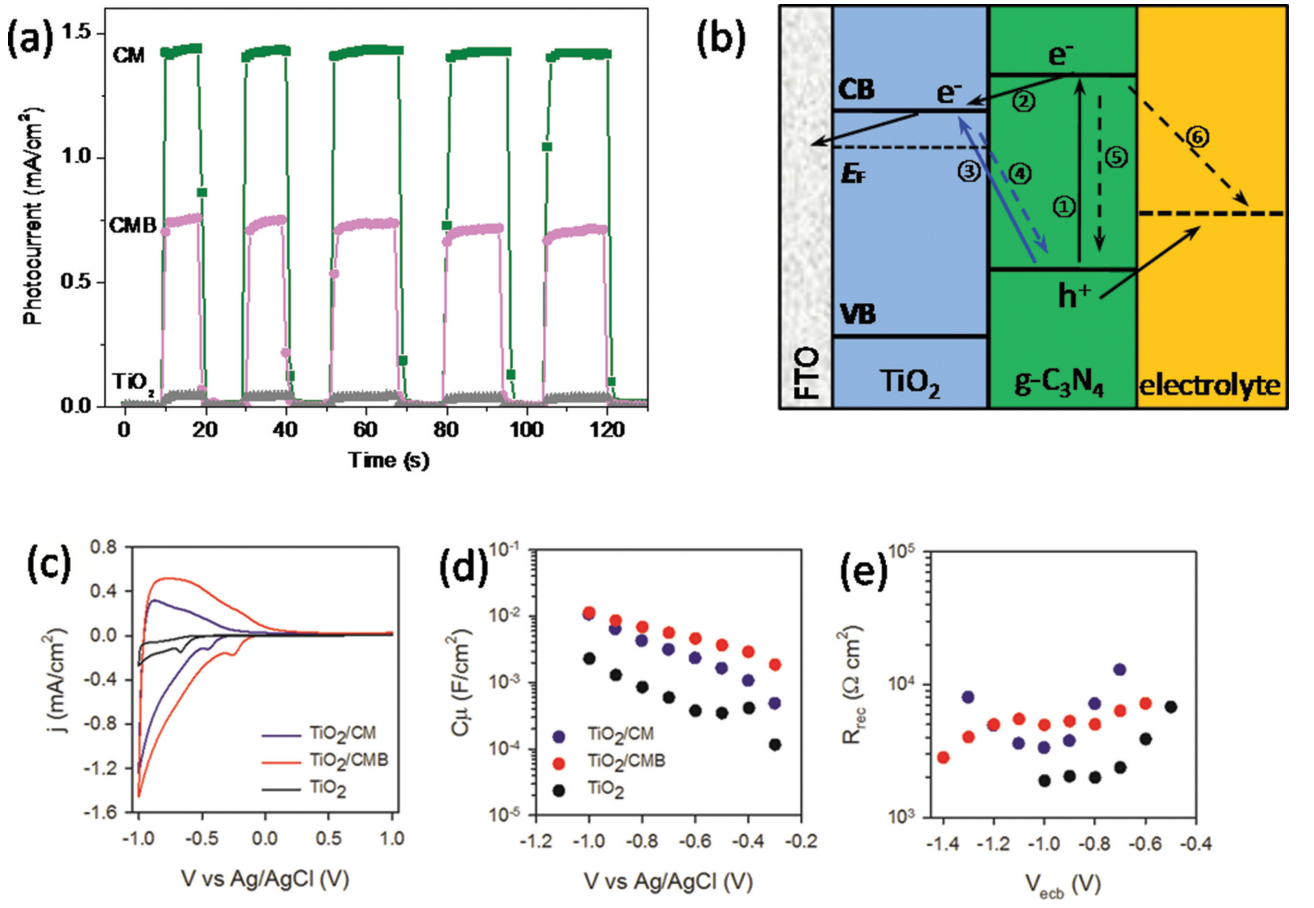

Figure 4. a) Photocurrent response of pristine TiO_2, TiO_2/CM, and TiO_2/CMB substrates under white light ($\lambda > 410$ nm). The measurement was carried out in a three-electrode system, Pt as the counter and Ag/AgCl as the reference electrode and 0.1 M Na_2S solution as the electrolyte. The light was chopped manually. b) Schematic energy diagrams in the TiO_2/ C_3N_4 system under light excitation and the proposed charge transfer mechanism (path 1, 2, and 3, charge excitation and transfer; path 4, 5, and 6, charge recombination). c) Cyclic voltammetry, d) chemical capacitance (C_μ), and e) R_{rec} of pristine TiO_2, TiO_2/CM, and TiO_2/CMB substrates obtained in the dark.

Adv. Optical Mater. **2015**,
DOI: 10.1002/adom.201500010

light illumination ($\lambda > 410$ nm) using a typical three-electrode setup in Na_2S (0.1 M) aqueous solution without applying bias. As expected, the pristine TiO_2 showed low photocurrent (0.045 mA cm^{-2}) because of its poor visible-light absorption. The photoactivity was significantly enhanced for TiO_2/CM and the photocurrent reached 1.4 mA cm^{-2}, mostly related to the improved light absorption and to the recombination inhibition as will show later in the manuscript. The photocurrent decreased to 0.7 mA cm^{-2} for TiO_2/CMB although it showed further enhanced light absorbance. The decrease of the photocurrent is probably due to higher defects levels (because of a too high carbon doping) which can result in higher recombination of charge carriers. In order to further study the photoactivity of carbon nitride, we measured the photocurrent versus the light intensity (Figure S10, Supporting Information). The photocurrent profile showed a typical solar cell behavior and can be well fitted into a linear model for both TiO_2/CM and TiO_2/CMB. Furthermore, we note that the photocurrent profiles can be divided into two parts, namely the current increased more quickly at low light intensity (<2000 μmol m^{-2} s^{-1}) than at higher light intensity (up to 20000 μmol m^{-2} s^{-1}). This can be understood due to the enhanced recombination of the photogenerated charge carriers at high illumination intensities.[20] The TiO_2/C_3N_4 substrates also illustrated considerable photocurrent under blue light (465 nm), i.e., 0.65 and 0.24 mA cm^{-2} for TiO_2/CM and TiO_2/CMB (Figure S11, Supporting Information), while pristine TiO_2 did not show any noticeable photoresponse. Besides, the hydrophilicity of TiO_2 substrate was checked before and after C_3N_4 sensitization and there was no obvious change based on contact angle measurement (Figure S12, Supporting Information), indicating the improvement of photocurrent should be ascribed to modified electronic/optical properties.

Combining with the chemical coupling between TiO_2 and C_3N_4 as revealed by XPS alongside the unique absorption spectra, we suppose that a novel, interface bound energy transition was created in this system. Normally speaking, upon absorption of light with energy higher than 2.7 eV (bandgap of C_3N_4), electrons in the ground state (HOMO) of C_3N_4 are excited to the conduction band and are relaxing to the lowest unoccupied molecular orbital (LUMO). From there, they usually transfer to the TiO_2 conduction band (CB) due to the difference in energy (path 1 and 2, Figure 4b).[18,21] The thermodynamically favorable electron injection is thereby driving charge separation. Subsequently, the negative charges transport through the TiO_2 nanoparticles and reach the conducting transparent electrode, while holes transfer to the electrolyte. In the present case, however, we suggest that the strong electronic coupling enables hybridization between the two semiconductors, and new molecular orbitals are generated at the interface (Figure S13, Supporting Information), according to the molecular orbital theory.[22] We note that it differs from the conventional heterojunction due to the strong chemical coupling. Consequently, photoinduced charge transition can take place between the new levels (blue arrow), which have significantly narrower energy gap and thus results in optical absorption far beyond the bandgap of either C_3N_4 or TiO_2. This TiO_2/C_3N_4 can be considered as a joint electronic system and behaves in the way of charge-transfer complex. Similar phenomenon was previously observed in carbon@TiO_2 nanocomposite, wherein a "dyade" structure was suggested to describe the properties.[23]

Furthermore, the electronic coupling can enable an alternative charge transfer (under illumination) from C_3N_4 HOMO directly into the unoccupied states in TiO_2 CB[24] (path 3, Figure 4b). This kind of transfer has also been demonstrated between TiO_2 and other sensitizers such as catechol.[25] However, one of the key issues arising from this transition is the fast recombination at the interface of TiO_2/C_3N_4, induced by the electron transition back from the metal oxide to the C_3N_4 (path 4, Figure 4b) which would severely diminish the photocurrent. This can explain the relatively low photocurrent obtained from TiO_2/C_3N_4 system compared with standard sensitized solar cells (≈10 mA cm^{-2}),[25,26] although the absorption was strongly extended to the visible light range. Moreover, the obtained photovoltage (Figure S14, Supporting Information) in the C_3N_4/TiO_2 cell is relatively low (≈170 mV). The photovoltage in PEC is the energy gap between the TiO_2 Fermi level (electrons) and the chemical potential of the electrolyte (holes) and for the normal TiO_2 PEC cell in Na_2S electrolyte the photovoltage is ≈300 mV.[26] The decreased photovoltage can be explained by (1) the downshift of the TiO_2 energy level with respect to the electrolyte (2) the high recombination rate limits the electron concentration in the TiO_2 (3) the negative potential of the Na_2S electrolyte.

A deeper analysis of the photoelectrochemical behavior of the TiO_2/C_3N_4 heterostructures was carried out by means of cyclic voltammetry and impedance spectroscopy. Figure 4c shows the cyclic voltammetry curves obtained for both CM and CMB-modified TiO_2 substrates and the comparison with pristine TiO_2 electrodes. These curves show the classical capacitive behavior of TiO_2 under cathodic bias related to the increased density of states as we approach the conduction band of the material. In addition, the reduction peak (at –0.6 V vs Ag/AgCl for pristine TiO_2), which reflects electron transfer from the TiO_2 CB to localized surface/trap state was clearly shifted for the C_3N_4-modified TiO_2 substrates to more positive potentials, underlining the existence of new electron transfer mechanisms in the dyadic material.[27] In order to characterize this shift further, electrochemical impedance spectroscopy (EIS) in dark was carried out. Figure S15 (Supporting Information) shows an example of the complex plane plots recorded on the tested samples. The obtained impedance spectra were fitted by using the well-known models applied to liquid DSSCs.[28] The adapted model employed in the present study is shown as Figure S16 (Supporting Information). The extracted chemical capacitance for TiO_2, C_μ, is plotted in Figure 4d as a function of the reference electrode potential and monitors the exponential density of states of TiO_2 below the conduction band.

The slope of the C_μ versus the potential in the semi-logarithmic scale is similar for all the electrodes, which indicates that the sensitization with C_3N_4 does not significantly modify the density of interband states of TiO_2. However, a clear anodic shift of about ≈200 mV is observed for C_μ of the C_3N_4-sensitized TiO_2 electrodes. The anodic shift (increase of capacitance at the same voltage) can be attributed to (1) downshift of the energy bands (Figure S17a, Supporting Information) with respect to the electrolyte due to the exponential distribution of the electronic states in TiO_2 (more states are exposed to the electrolyte) or (2) distribution broadening of the TiO_2 density of states (Figure S17b, Supporting Information). However,

based on the slopes of capacitance versus potential, we can exclude the band broadening, further proving the strong electronic interactions between the materials. Figure 4f shows the recombination resistance (R_{rec}), of electrons in the conduction band of TiO_2 with accepting species in the electrolyte (we note that in the TiO_2/C_3N_4 recombination rates cannot be obtained by this measurement). In order to compare the R_{rec} among different samples, we have corrected the applied voltage to a common equivalent conduction band, (V_{ecb}) in order to analyze this parameter on the basis of a similar density of electrons (i.e., the same distance between the electron Fermi level and TiO_2 CB), since R_{rec} depends on the density of electrons in the TiO_2 CB.[29] The lowest R_{rec} values are obtained for pristine TiO_2 and the highest ones for the TiO_2/CM electrode (i.e., the lowest recombination rate), indicating that C_3N_4 obtained with the CM precursor inhibits the charge recombination from the TiO_2 to the electrolyte. However, the R_{rec} for TiO_2/CMB is lower compared with TiO_2/CM, except for a small interval of approximately 300 mV, and approaches that of pristine TiO_2 at the highest applied voltages tested in the present study, which explains well the lower photocurrent found and showed in Figure 4a.

In conclusion, a study of carbon nitride as a potential stable solid-state sensitizer for TiO_2 electrodes with a novel dyade-type structure for improved visible-light activity is reported. The synthesis carried out by in situ, vapor transport growth of C_3N_4 coatings onto the nanoparticles of TiO_2 mesoporous thin film produced a strong chemical coupling, indicated by the generation of a direct Ti–O–C bond. This bonding enabled creation of additional molecular orbitals at the interface, resulting in a strong red-shift of the optical absorption. The chemical and photophysical properties of the new hybrid materials were further investigated by EIS, confirming that C_3N_4 acts as a surface dipole structure downshifting the energy levels over the TiO_2 surface. We strongly believe that this work opens new possibilities to achieve more efficient C_3N_4-based photocatalysts and electrochemical cells by optimizing the electron communication between the organic semiconductor and the supporting metal oxide substrate alongside the hole acceptor. Moreover, the fundamental understandings on the photophysical properties and the chemical interactions provide the opportunity to design refined types of communicating hybrid systems, such as nitrogen doped carbon at metal oxides.

Supporting Information

Supporting Information is available from the Wiley Online Library or from the author.

Acknowledgements

M.S. thanks "Minerva Fellowship" for financial support.

Received: January 5, 2015
Revised: March 5, 2015
Published online:

[1] a) Y. Zheng, Y. Jiao, J. Chen, J. Liu, J. Liang, A. Du, W. Zhang, Z. Zhu, S. C. Smith, M. Jaroniec, *J. Am. Chem. Soc.* **2011**, *133*, 20116; b) Y. Zheng, Y. Jiao, Y. Zhu, L. H. Li, Y. Han, Y. Chen, A. Du, M. Jaroniec, S. Z. Qiao, *Nat. Comm.* **2014**, *5*, 3783.
[2] X. Zhang, X. Xie, H. Wang, J. Zhang, B. Pan, Y. Xie, *J. Am. Chem. Soc.* **2012**, *135*, 18.
[3] J. Xu, T. J. K. Brenner, L. Chabanne, D. Neher, M. Antonietti, M. Shalom, *J. Am. Chem. Soc.* **2014**, *136*, 13486.
[4] a) S. Yan, Z. Li, Z. Zou, *Langmuir* **2009**, *25*, 10397; b) Q. Li, B. Yue, H. Iwai, T. Kako, J. Ye, *The J. Phys. Chem. C* **2010**, *114*, 4100; c) L. Ge, F. Zuo, J. Liu, Q. Ma, C. Wang, D. Sun, L. Bartels, P. Feng, *J. Phys. Chem. C* **2012**, *116*, 13708.
[5] X. C. Wang, K. Maeda, X. F. Chen, K. Takanabe, K. Domen, Y. D. Hou, X. Z. Fu, M. Antonietti, *J. Am. Chem. Soc.* **2009**, *131*, 1680.
[6] G. Liu, P. Niu, C. Sun, S. C. Smith, Z. Chen, G. Q. Lu, H.-M. Cheng, *J. Am. Chem. Soc.* **2010**, *132*, 11642.
[7] a) Y. S. Jun, E. Z. Lee, X. Wang, W. H. Hong, G. D. Stucky, A. Thomas, *Adv. Funct. Mater.* **2013**, *23*, 3661; b) M. Shalom, S. Inal, C. Fettkenhauer, D. Neher, M. Antonietti, *J. Am. Chem. Soc.* **2013**, *135*, 7118.
[8] Y. Zheng, J. Liu, J. Liang, M. Jaroniec, S. Z. Qiao, *Energy Environ. Sci.* **2012**, *5*, 6717.
[9] Y. Hou, Z. Wen, S. Cui, X. Guo, J. Chen, *Adv. Mater.* **2013**, *25*, 6291.
[10] S.-W. Cao, X.-F. Liu, Y.-P. Yuan, Z.-Y. Zhang, Y.-S. Liao, J. Fang, S. C. J. Loo, T. C. Sum, C. Xue, *Appl. Catal., B* **2014**, *147*, 940.
[11] H. Katsumata, T. Sakai, T. Suzuki, S. Kaneco, *Ind. Eng. Chem. Res.* **2014**, *53*, 8018.
[12] a) M. Shalom, S. Gimenez, F. Schipper, I. Herraiz-Cardona, J. Bisquert, M. Antonietti, *Angew. Chem. Int. Ed.* **2014**, *53*, 3654; b) J. S. Zhang, X. F. Chen, K. Domen, J. D. Epping, X. Z. Fu, M. Antonietti, X. C. Wang, *Angew. Chem. Int. Ed* **2010**, *49*, 441; c) M. Shalom, M. Guttengag, C. Fettkenhauer, S. Inal, D. Neher, A. Liobet, M. Antoniettie, *Chem. Mater.* **2014**, *26*, 5812; d) D. Chen, K. Wang, T. Ren, H. Ding, Y. Zhu, *Dalton Trans.* **2014**, *43*, 13105.
[13] A. Thomas, A. Fischer, F. Goettmann, M. Antonietti, J.-O. Muller, R. Schlogl, J. M. Carlsson, *J. Mater. Chem.* **2008**, *18*, 4893.
[14] T. Ohsaka, F. Izumi, Y. Fujiki, *J. Raman Spectrosc.* **1978**, *7*, 321.
[15] F. Yang, M. Lublow, S. Orthmann, C. Merschjann, T. Tyborski, M. Rusu, S. Kubala, A. Thomas, R. Arrigo, M. Hävecker, T. Schedel-Niedrig, *ChemSusChem* **2012**, *5*, 1227.
[16] J. Hu, P. Yang, C. M. Lieber, *Phys. Rev. B* **1998**, *57*, R3185.
[17] a) B. Chai, T. Peng, J. Mao, K. Li, L. Zan, *Phys. Chem. Chem. Phys.* **2012**, *14*, 16745; b) J. Wang, W.-D. Zhang, *Electrochim. Acta* **2012**, *71*, 10; c) N. Boonprakob, N. Wetchakun, S. Phanichphant, D. Waxler, P. Sherrell, A. Nattestad, J. Chen, B. Inceesungvorn, *J. Colloid Interface Sci.* **2014**, *417*, 402; d) L. Zhang, D. Jing, X. She, H. Liu, D. Yang, Y. Lu, J. Li, Z. Zheng, L. Guo, *J. Mater. Chem. A* **2014**, *2*, 2071.
[18] X.-J. Wang, W.-Y. Yang, F.-T. Li, Y.-B. Xue, R.-H. Liu, Y.-J. Hao, *Ind. Eng. Chem. Res.* **2013**, *52*, 17140.
[19] a) Z. Lin, A. Orlov, R. M. Lambert, M. C. Payne, *J. Phys. Chem. B* **2005**, *109*, 20948; b) L.-W. Zhang, H.-B. Fu, Y.-F. Zhu, *Adv. Funct. Mater.* **2008**, *18*, 2180.
[20] C. O. Kim, S. W. Hwang, S. Kim, D. H. Shin, S. S. Kang, J. M. Kim, C. W. Jang, J. H. Kim, K. W. Lee, S.-H. Choi, E. Hwang, *Sci. Rep.* **2014**, *4*, 5603.
[21] Y. Chen, W. Huang, D. He, Y. Situ, H. Huang, *ACS Appl. Mater. Interfaces* **2014**, *6*, 14405.
[22] G. Li, R. Zhu, Y. Yang, *Nat. Photonics* **2012**, *6*, 153.

[23] L. Zhao, X. Chen, X. Wang, Y. Zhang, W. Wei, Y. Sun, M. Antonietti, M.-M. Titirici, *Adv. Mater.* **2010**, *22*, 3317.

[24] a) F. De Angelis, S. Fantacci, E. Mosconi, M. K. Nazeeruddin, M. Grätzel, *J. Phys. Chem. C* **2011**, *115*, 8825; b) N. J. Cherepy, G. P. Smestad, M. Grätzel, J. Z. Zhang, *J. Phys. Chem. B* **1997**, *101*, 9342.

[25] I. Hod, M. Shalom, Z. Tachan, S. Rühle, A. Zaban, *J. Phys. Chem. C* **2010**, *114*, 10015.

[26] Y.-L. Lee, B.-M. Huang, H.-T. Chien, *Chem. Mater.* **2008**, *20*, 6903.

[27] S. Giménez Juliá, H. K. Dunn, P. Rodenas, F. Fabregat Santiago, S. G. Miralles, E. M. Barea Berzosa, R. Trevisan, A. Guerrero Castillejo, J. Bisquert, *J. Electroanal. Chem.* **2012**, *668*, 119.

[28] a) F. Fabregat-Santiago, J. Bisquert, G. Garcia-Belmonte, G. Boschloo, A. Hagfeldt, *Sol. Energy Mater. Sol. Cells* **2005**, *87*, 117; b) F. Fabregat-Santiago, G. Garcia-Belmonte, J. Bisquert, A. Zaban, P. Salvador, *J. Phys. Chem. B* **2001**, *106*, 334.

[29] a) V. González-Pedro, X. Xu, I. Mora-Seró, J. Bisquert, *ACS Nano* **2010**, *4*, 5783; b) A. Braga, S. Giménez, I. Concina, A. Vomiero, I. n. Mora-Seró, *J. Phys. Chem. Lett.* **2011**, *2*, 454.